Heat and Moisture Budget Analyses Using BOMEX Data

TSUYOSHI NITTA AND STEVEN ESBENSEN

Department of Meteorology, University of California, Los Angeles, 90024

(Manuscript received 22 March 1973, in revised form 13 September 1973)

ABSTRACT

Large-scale heat and moisture budgets over the tropical Atlantic Ocean are examined during Phase 3 (22–30 June 1969) of the Barbados Oceanographic and Meteorological Experiment (BOMEX). From the satellite cloud photographs of ATS-3, the analyzed period is subdivided into an undisturbed part and a disturbed part. During the undisturbed period, downward motion predominates from the surface to about 500 mb and a large apparent heat sink and apparent moisture source are found near the top of the trade inversion layer. The upward heat flux due to cumulus clouds is confined below the 700-mb level. On the other hand during the relatively disturbed period, upward motion takes place at low levels and the heat flux due to cumulus convection extends to at least 500 mb. Values of the total heat flux estimated by large-scale budgets agree well with those obtained independently by bulk aerodynamic computations.

1. Introduction

It is well known that cumulus clouds are very often associated with large-scale wave disturbances and organized into cloud clusters (Joint Organizing Committee Study Group, 1970; Chang, 1970). Recent studies by Manabe *et al.* (1970), Nitta (1970, 1972), and Wallace (1971) showed the importance of the released latent heat of cumulus convection for large-scale tropical disturbances.

Large-scale mass, heat, and moisture budgets over the western Pacific region have been analyzed by many authors. Williams (1970) showed the marked differences between the large-scale budgets of cloud clusters and clear areas. Tropical cloud clusters typically exhibit cyclonic shear in the lower troposphere, deep tropospheric convergence and large vertical mass transport. Reed and Recker (1971) and Nitta (1972) obtained a large apparent heat source in the middle and upper troposphere over the Marshall Islands. Recently Yanai *et al.* (1973) diagnostically determined the bulk properties of tropical clusters from the large-scale heat and moisture budgets using a simple model of a cumulus ensemble. They demonstrated that the cloud mass flux far exceeds the mean vertical mass flux and that the large-scale heating of the environment is primarily due to its adiabatic compression in the compensating downward motion. They also showed the importance of the cooling effects due to re-evaporation of liquid water detrained from the clouds. Gray (1972) analyzed large-scale budgets statistically and obtained the same conclusions.

Meanwhile, Holland and Rasmusson (1973) and Augstein *et al.* (1973) analyzed the budgets over the Atlantic trade wind region specifically during undisturbed periods. Their results of mass, heat and moisture budgets are very different from those obtained over the active ITCZ region in the western Pacific. During the undisturbed period, a strong trade inversion exists near 800 mb and substantial sub-grid scale eddy moisture flux is confined below the inversion.

The main purpose of this study is to demonstrate the difference of large-scale heat and moisture budgets between two different large-scale situations within a trade wind regime, an undisturbed period and a disturbed period, from the point of view of interaction between large-scale fields and cumulus convection. Not only the large-scale budgets but also the manner of the interaction between the large-scale fields and the cumulus convection may differ in different regions and in different large-scale situations.

2. Data

BOMEX was conducted during May, June, and July 1969. In this study we use the rawinsonde, ship boom, and radiometersonde data for Phase 3 from 22 to 30 June. The rawinsonde and ship boom data were provided by Dr. E. Rasmusson and Mr. J. Ching at the Center for Experiment Design and Data Analysis (CEDDA) of NOAA.

Fig. 1 shows the fixed ship locations during the period considered. The rawinsonde data set consists of the soundings taken at each of the four corner ships—the *Rainier*, the *Mount Mitchell*, the *Discoverer*, and the *Oceanographer*. Measurements of temperature, humidity, and wind speed and direction are available 15 times per day. With the exception of the 0000 GMT and 0300 GMT observations, the time interval between soundings is 1½ hours. The observations extend from

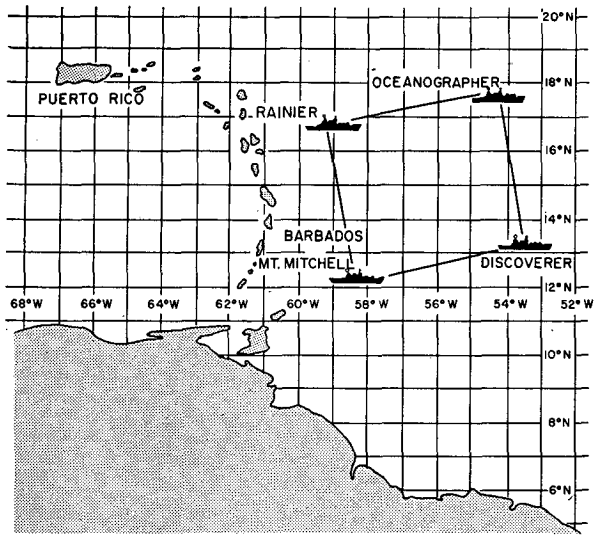

FIG. 1. BOMEX fixed-ship array during Phases 1, 2 and 3.

the sea surface to 500 mb above the surface with a vertical resolution of 10 mb. Original data whose values were more than three standard deviations from the mean at each level were discarded. Then missing data were linearly interpolated in the vertical if possible. If not, the interpolation was performed in time. For computations of large-scale mass, heat, and moisture budgets, we used weighted averaged rawinsonde data with a 20-mb interval. The daytime humidity errors in the rawinsonde data due to radiative heating of the hygristor element (see Teweles, 1970) were corrected using a curve suggested by Ostapoff *et al.* (1970) regardless of the cloud cover even though this is an oversimplification of the problem.

The fixed ship boom data set consists of observations of air temperature, specific humidity, and wind velocity at approximately 10 m above sea surface, and the sea surface temperature measured by a floating probe tethered immediately underneath the boom. The data received at UCLA were time series of hourly averaged values edited from the original 30-sec time series.

The radiation data set consists of a single average profile of total radiative heating obtained by Dr. S. Cox and used by Holland and Rasmusson (1973). See Fig. 8.

3. Method of analysis

Methods used in this study for computation of large-scale mass, heat, and moisture budgets are similar to to those used by Yanai *et al.* (1973). We use a p^*-coordinate system where $p^*=p_s-p$ (p_s is surface pressure).

The area-averaged vertical p^*-velocity, ω^*, is obtained from the equation of mass continuity

$$\overline{\nabla\cdot\mathbf{V}}+\frac{\partial\bar{\omega}^*}{\partial p^*}=0, \tag{1}$$

where over-bars denote area averages. The area-averaged horizontal divergence and relative vorticity over the BOMEX region are computed by

$$\overline{\nabla\cdot\mathbf{V}}=\frac{1}{A}\oint V_n dl \tag{2}$$

$$\bar{\zeta}=\frac{1}{A}\oint V_t dl, \tag{3}$$

where V_n and V_t are the normal and the tangential components of the winds along the periphery whose length is denoted by $\oint dl$ and A is the area of the region enclosed.

The equations of the first law of thermodynamics and moisture continuity averaged over the analyzed area are

$$\frac{c_p}{(p_0/p)^\kappa}\left(\frac{\partial\bar{\theta}}{\partial t}+\overline{\nabla\cdot(\theta\mathbf{V})}+\frac{\partial\overline{\theta\omega^*}}{\partial p^*}\right)=Q_R+L(c-e) \tag{4}$$

$$\frac{\partial\bar{q}}{\partial t}+\overline{\nabla\cdot(q\mathbf{V})}+\frac{\partial\overline{q\omega^*}}{\partial p^*}=e-c, \tag{5}$$

where θ is the potential temperature, q the mixing ratio, Q_R the heating rate due to radiation, c the rate of condensation per unit mass of air, e the rate of re-evaporation of cloud droplets, c_p the specific heat of air under constant pressure, $\kappa=R/c_p$, and L the latent heat of condensation. These equations can be rewritten

$$Q_1\equiv\frac{c_p}{(p_0/p)^\kappa}\left(\frac{\partial\bar{\theta}}{\partial t}+\overline{\nabla\cdot(\theta\mathbf{V})}+\frac{\partial\overline{\theta\omega^*}}{\partial p^*}\right)$$

$$=Q_R+L(c-e)-\frac{\partial\overline{s'\omega^{*\prime}}}{\partial p^*}, \tag{6}$$

$$Q_2\equiv-L\left(\frac{\partial\bar{q}}{\partial t}+\overline{\nabla\cdot(q\mathbf{V})}+\frac{\partial\overline{\theta\omega^*}}{\partial p^*}\right)=L(c-e)+L\frac{\partial\overline{q'\omega^{*\prime}}}{\partial p^*}, \tag{7}$$

where primes denote deviations from the areal averages and s is the dry static energy defined by

$$s\equiv c_pT+gz. \tag{8}$$

The dry static energy is the sum of enthalpy and potential energy. In Eqs. (6) and (7), it is assumed that subgrid-scale eddies in the horizontal components of wind have no significant correlatrions with θ, q and z, and $\overline{s'\omega^{*\prime}}$ and $\overline{q'\omega^{*\prime}}$ are vertical eddy transports of sensible heat and moisture due to subgrid-scale eddies, including both cumulus convection and turbulent motion in the boundary layer. The apparent heating, Q_1, and the apparent moisture sink, Q_2, of the large-scale motion system can be computed from large-scale operational rawinsonde data. Holland and Rasmusson

(1973) and Augstein *et al.* (1973) evaluated a profile of subgrid-scale vertical moisture flux as the residual of Eq. (7) neglecting the terms of condensation and evaporation. However, since the vertical profiles of condensation and evaporation are not in general equal with each other in the cloud layer even during undisturbed periods, the neglect of these terms results in incorrect estimates of the subgrid-scale vertical moisture flux. In this study we evaluate the eddy transport of total heat (latent heat plus sensible heat) instead of attempting to evaluate each heat transport separately.

From Eqs. (6) and (7), we obtain

$$Q_1-Q_2-Q_R=-\frac{\partial\overline{h'\omega^{*\prime}}}{\partial p^*}, \tag{9}$$

where h is the moist static energy defined by

$$h\equiv c_pT+gz+Lq. \tag{10}$$

The moist static energy is the sum of s and latent energy. The quantity $\overline{h'\omega^{*\prime}}$ is a measure of the vertical eddy transport of total heat due to cumulus convection in the free atmosphere and also due to turbulent eddies in the boundary layer. Note that the left-hand side of Eq. (9) does not include the terms of condensation and evaporation, so that we can obtain vertical eddy transport of total heat without artificial assumptions about these terms. If we integrate Eq. (9) from $p^*=500$ mb (upper boundary of the BOMEX observations) to p^* or from the surface to p^*, we obtain total heat flux at p^* defined by

$$F(p^*)\equiv\frac{1}{g}\overline{-h'\omega^{*\prime}}\Big|_{p^*}=F(500)+\frac{1}{g}\int_{p^*}^{500}(Q_1-Q_2-Q_R)dp^{*\prime}$$

$$=F(0)-\frac{1}{g}\int_0^{p^*}(Q_1-Q_2-Q_R)dp^{*\prime}, \tag{11}$$

where $F(0)$, $F(p^*)$ and $F(500)$ are the total heat fluxes at $p^*=0$, p^* and 500 mb, respectively. From Eq. (11) we obtain

$$F(0)-F(500)=\frac{1}{g}\int_0^{500}(Q_1-Q_2-Q_R)dp^*. \tag{12}$$

Unless the flux at the surface or $p^*=500$ mb is known, only the difference between $F(0)$ and $F(500)$ can be obtained. To obtain $F(p^*)$ we must know or assume $F(0)$ or $F(500)$. We have two methods of overcoming these difficulties. First, the total heat supply can be obtained from the ship boom data by using the bulk aerodynamic method. Second, in undisturbed situations where cumulus convection is confined below $p^*=500$ mb, it may be assumed that both the sensible and latent heat flux due to subgrid-scale eddies are zero at $p^*=500$ mb. If we make the additional assumption that the net condensation rate between the surface and $p^*=500$ mb is equal with the amount of precipitation P_0, the integrated Eqs. (6) and (7) are

$$\frac{1}{g}\int_0^{500}(Q_1-Q_R)dp^*=LP_0+S_0 \tag{13}$$

$$\frac{1}{g}\int_0^{500}Q_2dp^*=L(P_0-E_0), \tag{14}$$

where S_0 and E_0 are the supply of sensible heat and the rate of evaporation from the ocean surface. Using these relations, we can calculate the supply of sensible and latent heat from the ocean surface during undisturbed periods from the values of Q_1, Q_2 and Q_R, and observations of precipitation P_0.

4. Large-scale mass, heat, and moisture budgets

a. Classifications obtained from satellite

During the BOMEX periods, cloud photographs of ATS-3 were taken over the BOMEX area. Typical photographs near local noon at each day are shown in Fig. 2. These photographs are image enhancement, precision-display pictures of ATS-3 which were produced at the University of Wisconsin. The enhancement was designed to emphasize deep convective cores, land features, and small or thin clouds. By means of these cloud pictures, we subdivide Phase 3 of BOMEX into two parts. One, the period from 22 June to 26 June in which little active cumulus convection appears, we designate as the undisturbed period. Budget computations of moisture, heat, momentum, and energy during this undisturbed period were performed by Holland and Rasmusson (1973). The other, from 27 June to 29 June, is a period in which relatively active and organized convection develops over this area. During the period from late 28 June to early 29 June, an organized cloud cluster passes through the southern part of this area, as shown in Fig. 2G. Fig. 3 shows the time-height section of the vertical velocity. In Fig. 3, short period variations of less than 6 hr have been removed. During the whole period downward motion predominates. Within the dominant downward motion, diurnal variations are clearly seen. Such diurnal variations can also be found in other variables. A detailed analysis of the diurnal variations is presented by Nitta and Esbensen (1973).

Budget computations were carried out for each $1\frac{1}{2}$-hr observational time, but we shall only discuss mean budgets in this study. We first look at the difference in the mean heat and moisture budgets of the undisturbed period and the disturbed period. We then discuss the mean budgets for each day. Since there are no observations on 27 June, we computed the budget for the disturbed case by averaging the budgets of 28 June and 29 June.

b. Dry and moist static energy

Mean profiles of dry and moist static energy for the two periods are illustrated in Figs. 4A and 4B. Mean profiles of saturation moist static energy h^* are also shown; h^* is defined by

$$h^*=c_pT+gz+Lq^*(p,T), \tag{15}$$

where q^* is the saturation mixing ratio at temperature T. Using the definitions of s and h^*, it can be shown that

$$\frac{\partial s}{\partial z}\simeq c_p\left(\frac{p}{p_0}\right)^{R/c_p}\frac{\partial\theta}{\partial z} \tag{16}$$

and

$$\frac{\partial h^*}{\partial z}\simeq c_p\left(\frac{T}{\theta_e}\frac{\partial\theta_e}{\partial z}\right), \tag{17}$$

where $\theta_e\equiv\theta_d\exp(Lq^*/c_pT)$ is the equivalent potential temperature and θ_d is the partial potential temperature of dry air. Thus the vertical gradients of s and h^* give measures of the stability of dry air parcels and saturated air parcels, respectively. During the undisturbed period, dry static energy increases rather rapidly while moist static energy decreases sharply with increasing altitude within the layer between $p^*=160$ mb and $p^*=220$ mb. Also in this layer the saturated moist static energy increases with height. These results indicate that within this stable layer, a sharp decrease of moisture takes place. This stable layer corresponds to the trade inversion layer. Results obtained by Yanai *et al.* (1973) over the western Pacific ITCZ region show that there is no clearly defined stable layer in the lower troposphere as over this BOMEX area. Values of dry static energy are almost constant in the layer below $p^*=60$ mb and the level of $p^*=60$ mb may correspond to the top of the mixed layer. The structure of our undisturbed trade wind regime is nearly identical to that discussed by Malkus (1958).

During the disturbed period, the stable layer near $p^*=200$ mb is weakened. This weakness of stable layer may be caused by the upward energy transports due to active cumulus convection. In this period, the level

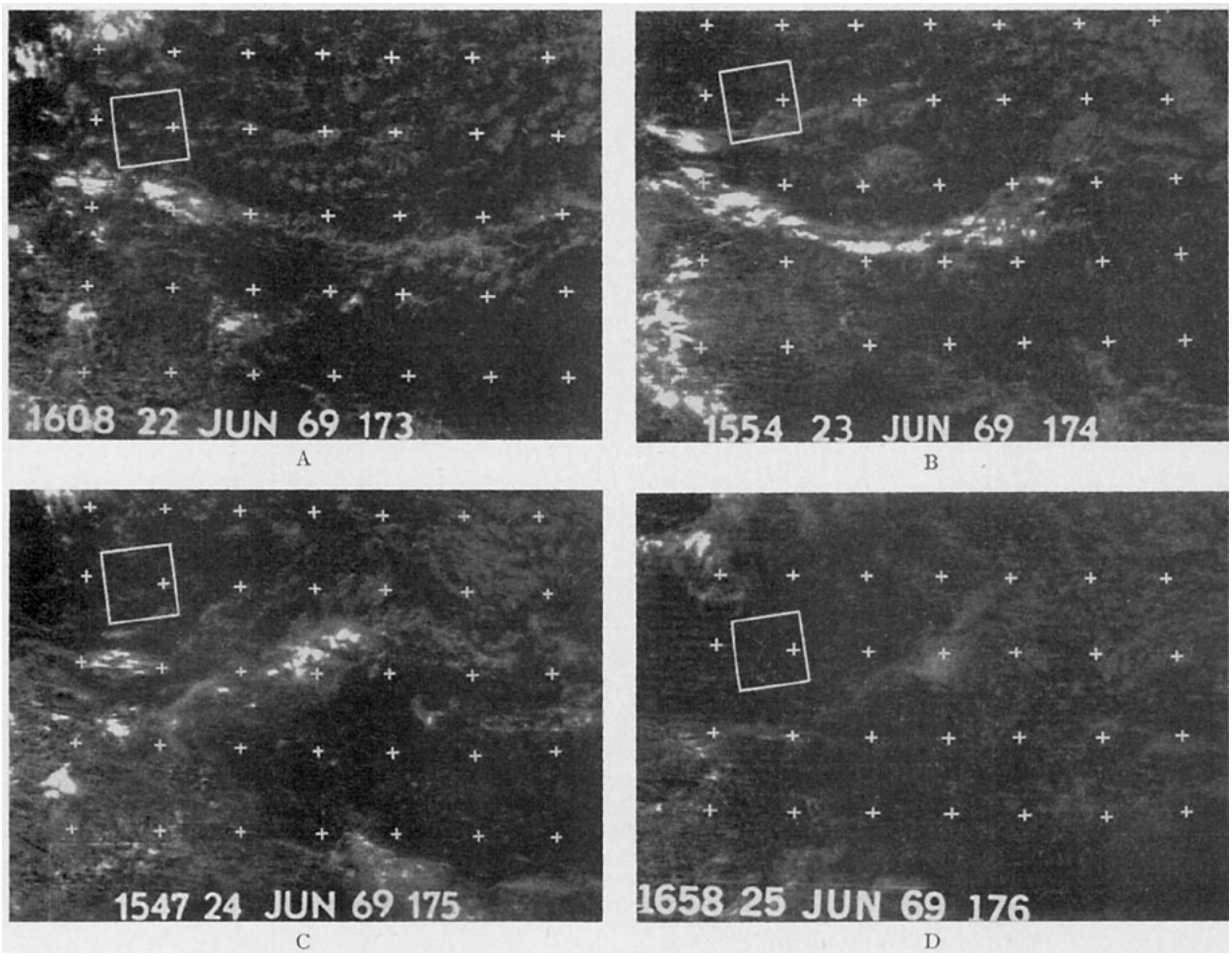

FIG. 2. ATS-3 image-enhancement, precision-display pictures for the period of June 22–29, 1969. The over-gridded box is a BOMEX square.

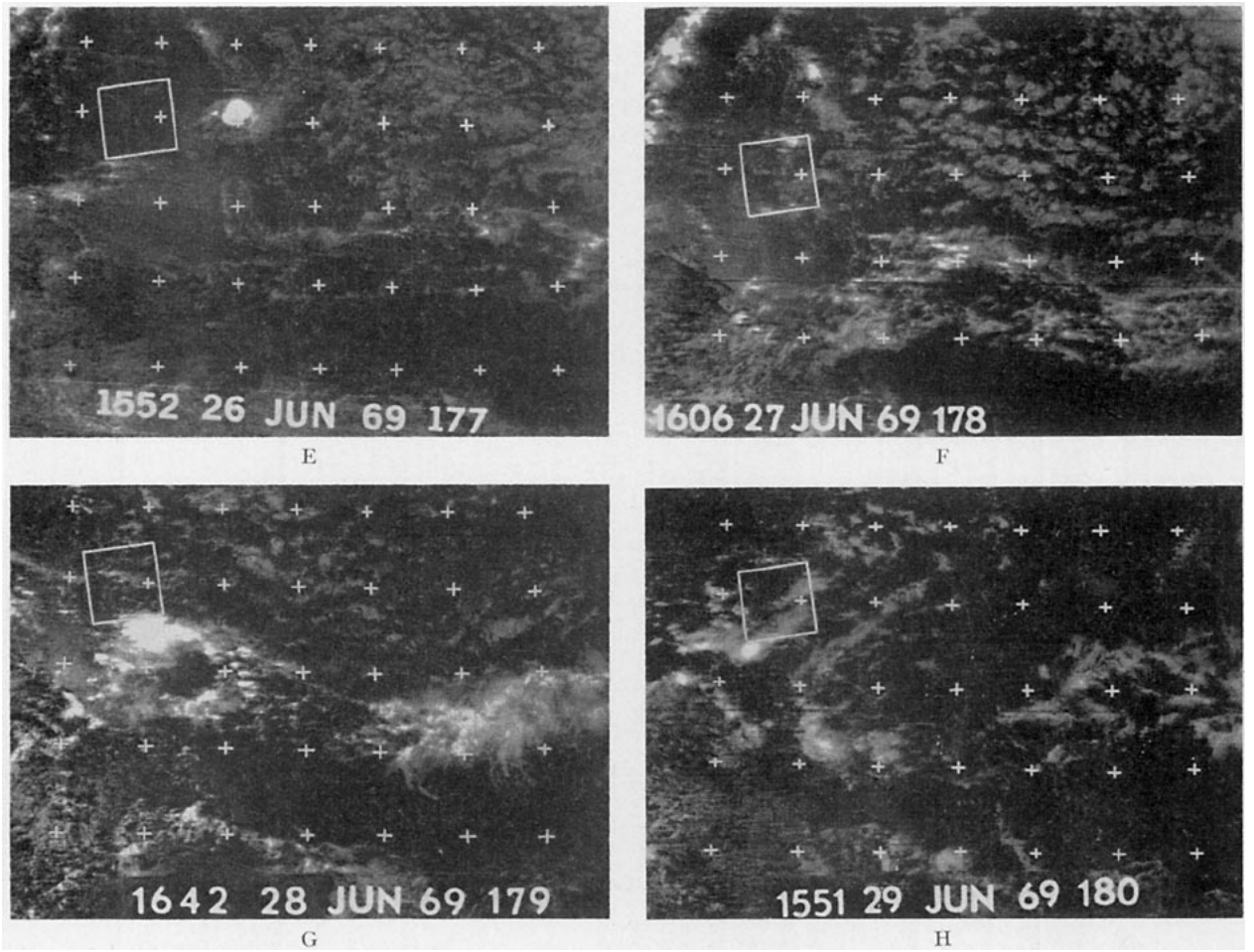

Fig. 2 (*continued*)

of $p^*=40$ mb may correspond to the height of the mixed layer, somewhat lower than in the undisturbed period.

c. *Divergence, vertical velocity, and vorticity*

The computed horizontal divergence profiles for the two periods are illustrated in Fig. 5. In the undisturbed period strong divergence occurs in the lower layer below $p^*=160$ mb, weak convergence exists in the middle layer from $p^*=160$ mb to $p^*=340$ mb and weak divergence takes place in the upper layer above $p^*=340$ mb. In contrast with the strong divergence in the lower layer for the undisturbed period, convergence exists in the lowest layer below $p^*=60$ mb during the disturbed period. Divergence is found aloft during the disturbed period but the magnitude of the divergence is smaller that that of the undisturbed period.

The vertical profiles of vertical velocity are shown in Fig. 6. In the undisturbed period downward motion predominates through the whole layer. Maximum downward motion occurs at $p^*=160$ mb. The vertical motion profile in the disturbed period is very different from that in the undisturbed period especially in the layer below $p^*=400$ mb. In this period, weak upward motion takes place in the lower layer below $p^*=120$ mb due to

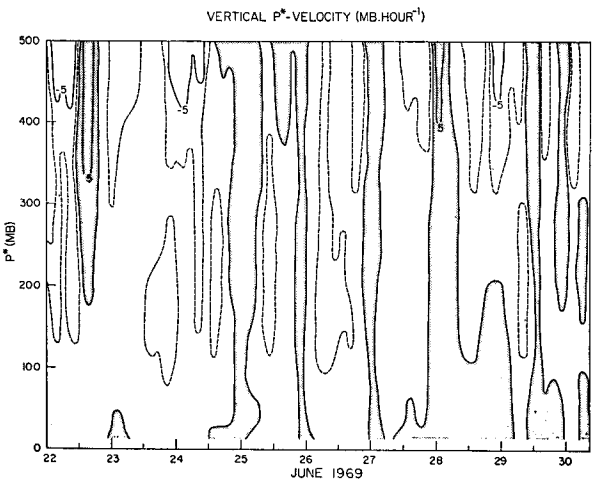

FIG. 3. Vertical p^*-velocity (ω^*) cross section. Shaded areas are upward motions.

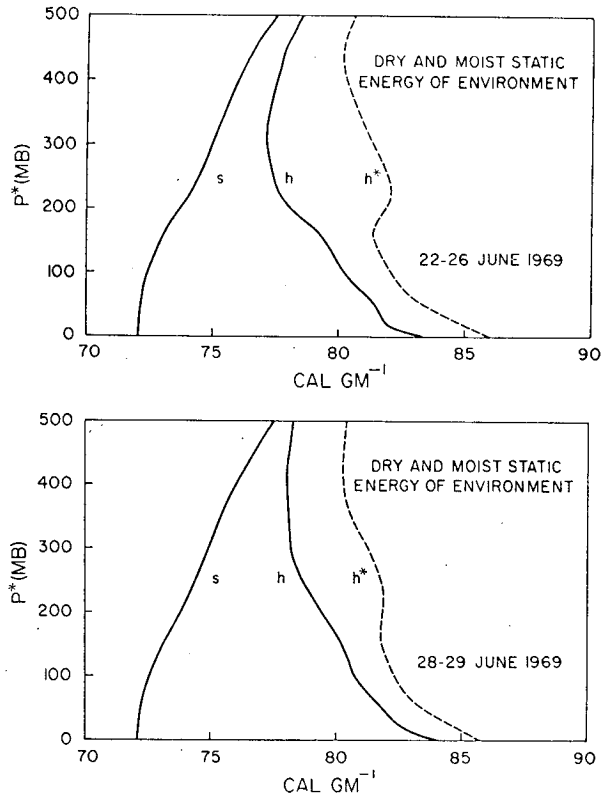

FIG. 4. Vertical profiles of dry static energy, moist static energy and saturation moist static energy for the undisturbed period 22–26 June (above) and the disturbed period 28–29 June (below).

the low-level convergence. Above that level downward motion predominates but the magnitude in the layer below $p^*=400$ mb is smaller than in the undisturbed case. The magnitude of downward motion above $p^*=400$ mb is almost the same as that of undisturbed case.

Fig. 7 shows the vertical profiles of relative vorticity. In the undisturbed period, the relative vorticity has large negative values through the whole layer. Relative vorticity in the disturbed period is larger than in the undisturbed period. Especially in the lower layer below $p^*=150$ mb the amount of relative vorticity is almost zero.

The difference of divergence, vertical velocity, and relative vorticity between the undisturbed period and the disturbed period can be clearly seen, especially in the lower layer. Characteristic features of the undisturbed period are low-level divergence, downward motion, and negative relative vorticity. These results agree with those obtained by Williams (1970) for clear sky case over the western Pacific region, and Holland and Rasmusson (1973) and Augstein *et al.* (1973) for undisturbed cases over the Atlantic trade region. The characteristic features of the disturbed period are convergence and upward motion in the lower layer. Large-scale analyses over the western Pacific ITCZ region obtained by Williams (1970), Reed and Recker (1971), Nitta (1972), and Yanai *et al.* (1973) showed that there is a deep layer of convergence up to about 10 km, a shallow layer of intense divergence aloft and large upward motion in the whole troposphere. Though the features of convergence and upward motion in the lower layer during the disturbed period over the BOMEX area are similar to those over the western Pacific region, the magnitude is much smaller and the depth of the layer is much thinner. Therefore, in spite of the existence of organized clusters during the disturbed period in this study, large-scale fields in this period are less disturbed compared with the western Pacific ITCZ region. Since large-scale fields on 28 June are more disturbed than those on 29 June, the characteristics of the disturbed case may appear more clearly on 28 June than the average of the two days. Budgets for each day are described later in this section.

d. Heat and moisture budgets

Apparent heat source and apparent moisture sink profiles for the two periods are shown in Fig. 8A and in Fig. 8B. Radiative heating is also shown in these figures. Since the final estimates of radiational cooling at each individual time have not been obtained, we use the averaged values of Q_R from 22 to 26 June obtained by Dr. S. Cox, which were also used by Holland and Rasmusson (1973).

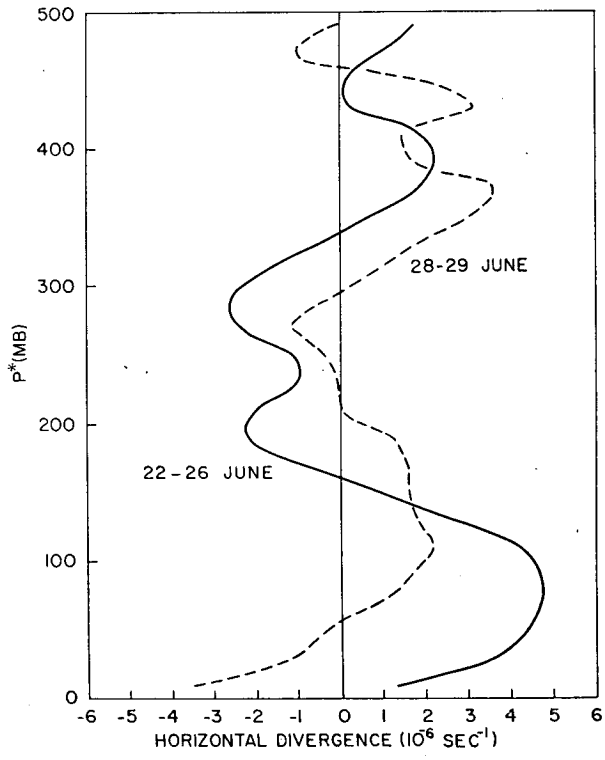

FIG. 5. Vertical profiles of horizontal divergence for the undisturbed period and the disturbed period.

In the undisturbed case, we obtain average values of Q_1 and Q_2 after we slightly adjust the original Q_1 and Q_2 for each day so that the total $F(p^*)$ for each day is never negative in the cloud layer. In addition, $F(500)$ is assumed to be zero. Near the top of the trade inversion layer ($p^*=200$ mb), we find a large apparent heat sink and apparent moisture source. These are probably caused by re-evaporation of cloud droplets which detrain near the top of the trade inversion. Above $p^*=250$ mb, the apparent heat sink and apparent moisture source decrease rapidly and tend to zero. The small values of Q_1 and Q_2 in the upper layer indicate that there are very few clouds which penetrate into the upper layer above the trade inversion layer. In the lower layer between $p^*=60$ mb (top of the mixed layer) and $p^*=160$ mb, there exists positive Q_1-Q_R, which may be caused by the adiabatic warming due to compensating downward motion in the environment between the cumulus clouds and negative Q_2 that may be mainly a result of detrainment from the clouds. Positive Q_1-Q_R and negative Q_2 below $p^*=60$ mb show the vertical convergence of eddy heat and moisture flux within the mixed layer.

In the disturbed period the vertical profiles of Q_1 and Q_2 are quite different from those during the undisturbed period. There is no strong apparent heat sink or moisture source at the level near $p^*=200$ mb as in the undisturbed period. In almost the whole layer between $p^*=40$ mb (top of the mixed layer) and $p^*=300$ mb, both Q_1-Q_R and Q_2 are positive mainly because of the compensating warming and drying effects of cumulus clouds. In the upper layer above $p^*=300$ mb, Q_1-Q_R and Q_2 become negative probably as the result of the detrainment effects of the clouds.

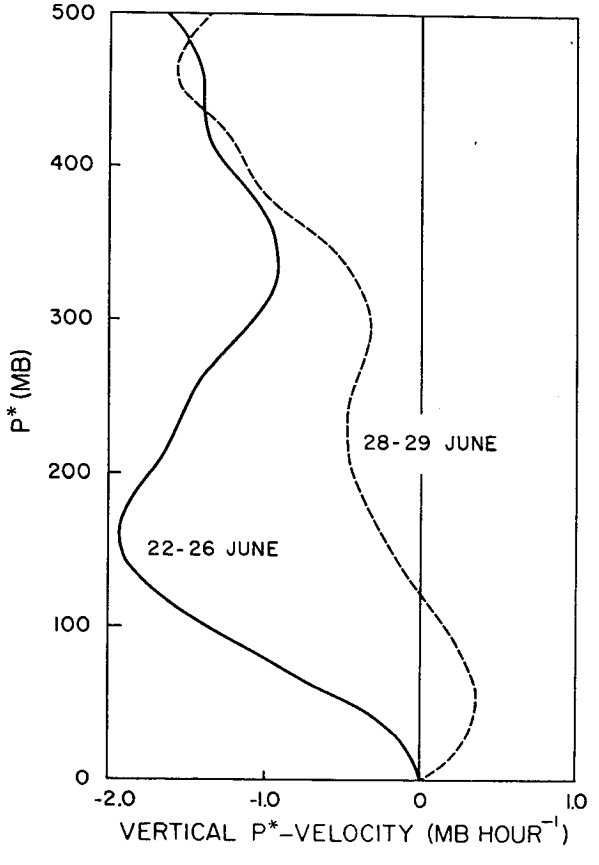

FIG. 6. Vertical profiles of vertical p^*-velocity for the undisturbed period and the disturbed period.

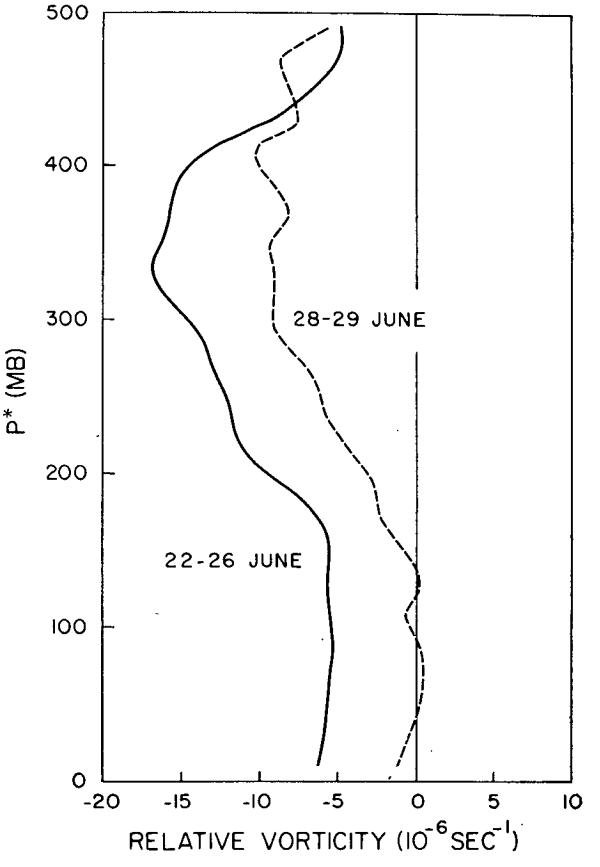

FIG. 7. Vertical profiles of relative vorticity for the undisturbed period and the disturbed period.

e. Budgets for each day

In the previous sub-section we discussed the mean budgets for the disturbed and undisturbed periods. However, large-scale heat and moisture budgets during each period vary from day to day. In this sub-section, we examine the day-to-day variations of the large-scale budgets.

Horizontal divergence, vertical velocity, relative vorticity, apparent heat source, and apparent moisture sink on individual days are shown in Figs. 9 to 12. During the period from 22 June to 24 June, the vertical profiles of $\nabla\cdot\mathbf{V}$, ω^*, ζ, Q_1 and Q_2 are generally the same and are similar to the mean profiles of the undisturbed case. Divergence is found in the lower layer below

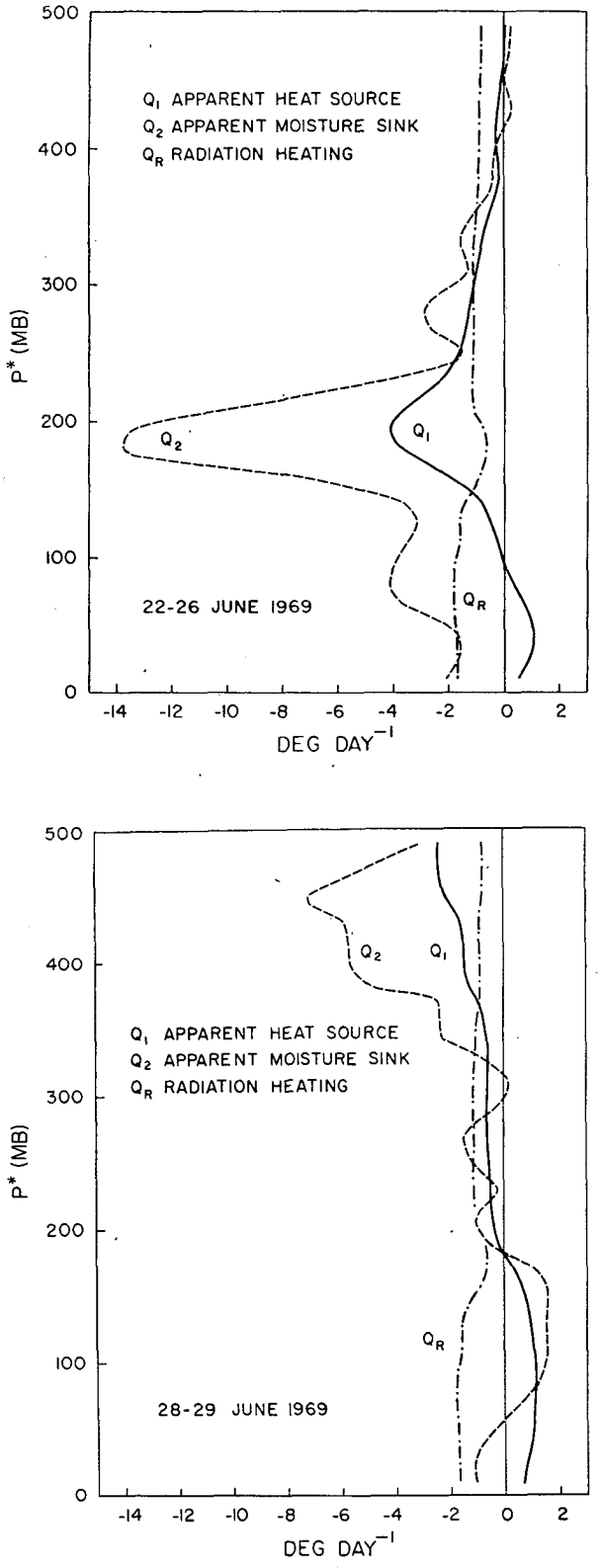

FIG. 8. Vertical profiles of apparent heat source, apparent moisture sink, and radiational heating for the undisturbed period (above) and for the disturbed period (below).

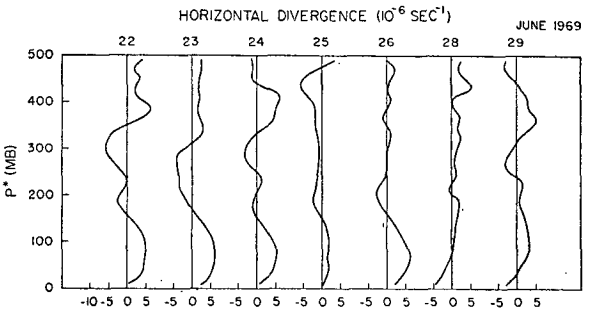

FIG. 9. Vertical profiles of horizontal divergence for each day.

$p^*=200$ mb and convergence occurs above that level. Strong downward motion and negative relative vorticity dominate the whole layer. Near the trade inversion layer, large apparent moisture sources and apparent heat sinks are found. Results on 26 June show similar characteristics to those of typical cases from 22 June to 24 June but the amplitudes are weaker. The results on 25 June are different from the others in the undisturbed period. From the synoptic weather maps produced by the National Hurricane Center, Miami (not shown), we find that the axis of an upper-level midlatitude trough lies directly over the BOMEX area and the effect of the trough extends down to 850 mb. The convergence, upward motion and positive relative vorticity found in the upper layer on 25 June are consistent with this feature. There is no large heat sink near the trade inversion layer.

From the satellite cloud photographs, it is found that cumulus clouds on 28 June are more active than those on 29 June. From the large-scale budget results, we can also say that 28 June is more disturbed than 29 June. On 28 June, upward motion takes place from the surface to $p^*=300$ mb due to low-level convergence. Positive relative vorticity occurs below $p^*=200$ mb. The apparent heat source and apparent moisture sink are found in the middle and lower layers below $p^*=300$ mb. Results on 29 June show characteristics of both the disturbed and undisturbed cases. Weak upward motion takes place in the thin layer below $p^*=80$ mb, but downward motion predominates in the upper layer and

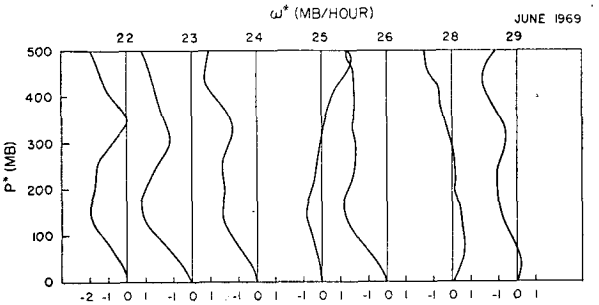

FIG. 10. Same as Fig. 9 for vertical p^*-velocity.

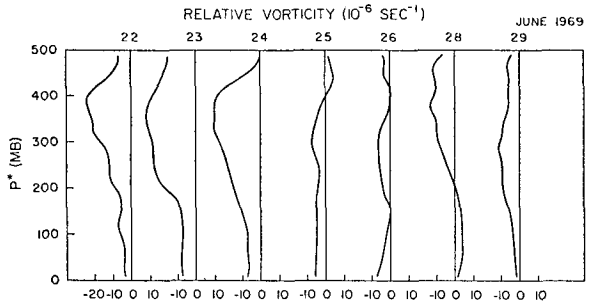

FIG. 11. Same as Fig. 9 for relative vorticity.

positive relative vorticity occurs in the whole layer. There exists an apparent heat source and an apparent moisture sink in the lower layer below $p^*=180$ mb and an apparent heat sink and an apparent moisture source in the upper layer above $p^*=340$ mb. These features are similar to those of 28 June. However, an apparent heat sink and apparent moisture source are found near the trade inversion layer as in the undisturbed cases although their amplitudes are smaller than in the undisturbed cases.

5. The vertical eddy flux of moist static energy

Figure 13 shows the vertical profiles of $F(p^*)-F(500)$ for the disturbed and undisturbed periods computed from Eq. (11) using the daily averaged values of Q_1-Q_R and Q_2. Since the vertical transport of moist

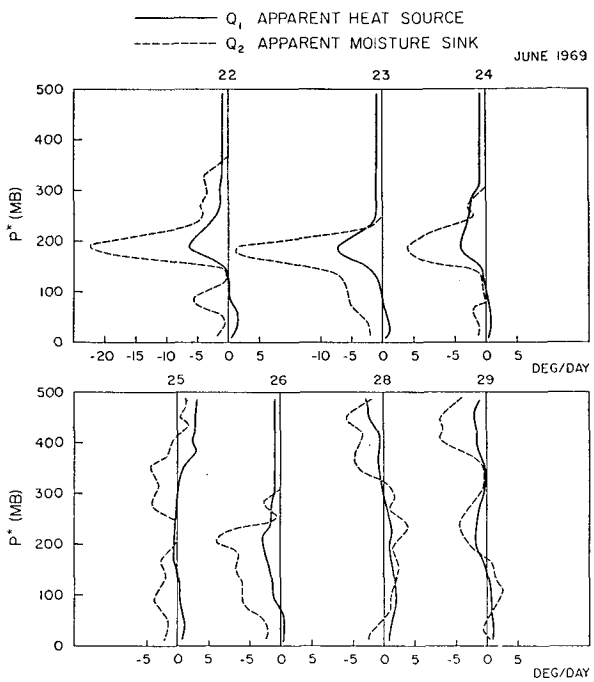

FIG. 12. Same as Fig. 9 for apparent heat source and apparent moisture sink.

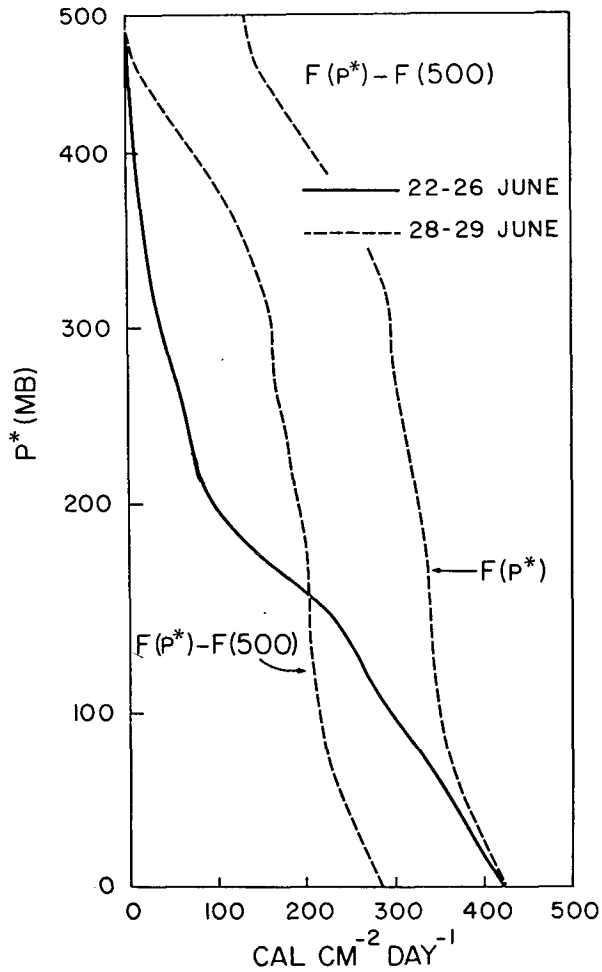

FIG. 13. Vertical profiles of $F(p^*)$–$F(500)$ for the undisturbed period and the disturbed period. The profile of $F(p^*)$ for the disturbed period is obtained by assuming that $F(0)$ for the disturbed period is roughly equal to $F(0)$ during the undisturbed period.

static energy by subgrid-scale eddies may be assumed to be negligible at $p^*=500$ mb in undisturbed situations, the profile for 22–26 June is just $F(p^*)$. We find that significant vertical eddy flux is confined below $p^*=300$ mb in the undisturbed period. The flux decreases gradually from its surface maximum to the top of the mixed layer at $p^*\sim60$ mb, decreases more rapidly to the $p^*=150$ mb level and then decreases very rapidly to the top of the trade wind inversion near 200 mb. At $p^*=300$ mb the flux is only 10% of its surface value. A profile of vertical eddy moisture flux presented by Holland and Rasmusson (1973) has a similar shape although their estimates below the inversion base are probably overestimated due to the neglect of condensation and evaporation.

During the relatively disturbed days of 28 and 29 June, $F(p^*)$ is significant over the entire 500 mb depth of the BOMEX box. The flux decreases gradually from

the sea surface maximum to the $p^*=80$ mb level. From this level to the $p^*=300$ mb level, the flux while decreasing remains nearly constant and then decreases to the 500-mb value.

The vertical profiles for individual days are shown in Fig. 14. During the undisturbed period all profiles have similar characteristics with the exception of 25 June. This profile is similar below $p^*=150$ mb but does not decrease rapidly above this level as do the other undisturbed profiles. The difference is due to the effect of the upper-level mid-latitude trough discussed in the previous section.

Using the mean precipitation of $P_0=0.2$ mm day^{-1} suggested by Holland and Rasmusson (1973) for the undisturbed period, we can obtain values of the sea surface supply of latent and sensible heat. Estimates of these values, the sea-to-air supply of moist static energy and the Bowen ratio are summarized in Table 1. These values are almost identical to those obtained by Holland and Rasmusson (1973).

During the disturbed period we cannot assume $F(500)=0$. Cumulus convection may penetrate the 500-mb level. The difference in eddy moist static energy

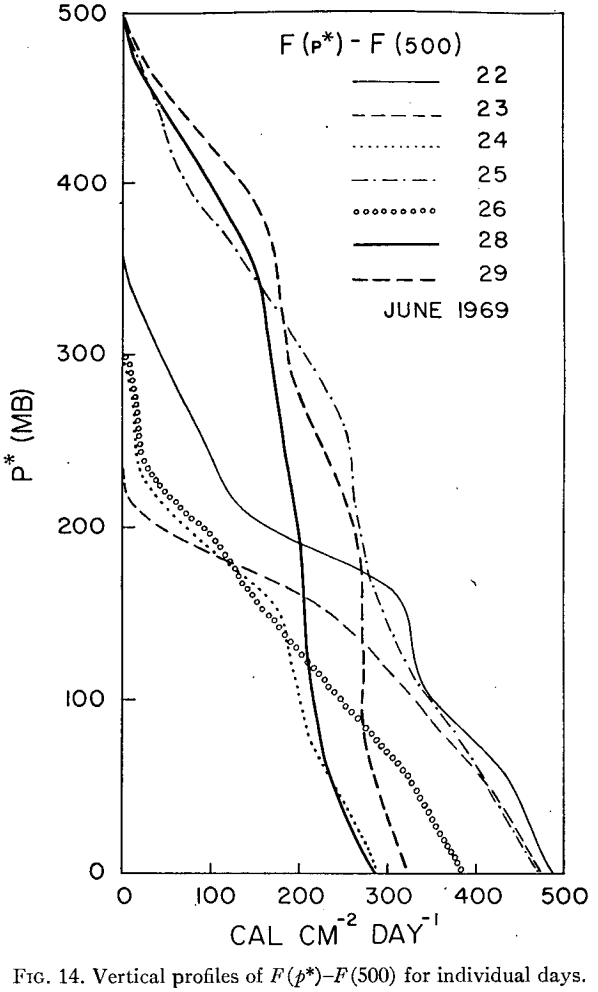

FIG. 14. Vertical profiles of $F(p^*)-F(500)$ for individual days.

TABLE 1. Heat and moisture budgets of undisturbed period.

$\frac{1}{g}\int_0^{500} Q_1 dp^*$	$\frac{1}{g}\int_0^{500} Q_2 dp^*$	$\frac{1}{g}\int_0^{500} Q_R dp^*$	LP_0
−95 ly day^{-1}	−372 ly day^{-1}	−143 ly day^{-1}	12 ly day^{-1}
S_0	LE_0	F_0	B
36 ly day^{-1}	384 ly day^{-1}	420 ly day^{-1}	0.094

transport between the surface and $p^*=500$ mb is 285 ly day^{-1}. This is 135 ly day^{-1} less than the supply from the surface in the undisturbed period. However, this does not mean that the sea surface supply is less during the disturbed period since cumulus convection may transport substantial static energy across the $p^*=500$ mb surface. We will return to this point later in the section.

The bulk aerodynamic method can be used to check the consistency of our budget computations during the undisturbed period, and to provide an estimate of $F(500)$ and hence $F(p^*)$ during the disturbed period. We note that

$$F(0)=-\frac{1}{g}\overline{h'\omega^{*\prime}}\Big|_{p^*=0} \doteq S_0+LE_0 \tag{18}$$

and

$$E_0=\rho c_q(q_0-q_a)V_a \tag{19}$$

$$S_0=B\cdot LE_0, \tag{20}$$

where ρ, c_q, q, V and B are the density of air in the surface layer, the empirical bulk aerodynamic coefficient for evaporation, specific humidity, absolute air velocity, and the Bowen ratio. The subscripts 0 and a refer to sea surface and anemometer level, respectively. We accept the suggestion of Pond *et al.* (1971) in setting $c_q=1.23\times10^{-3}$ and $B=0.1$ for the BOMEX periods which include our data set. The density and L are fixed at 1.15×10^{-3} gm cm^{-3} and 591 cal gm^{-1}, respectively. The calculated average evaporation over both periods is about 7 mm day^{-1}, which is slightly higher than the concensus values of 6 mm day^{-1} reported by Holland (1972) for Phase 3.

The comparison of $F(0)$ obtained by the bulk aerodynamic method and $F(0)-F(500)$ from the budget computations is shown in Fig. 15. During the undisturbed period 22–26 June, the agreement is quite good, meaning that $F(500)\approx0$. The lower values of $F(0)-F(500)$ during the disturbed period thus mean that the cumulus convection is resulting in the transport of nearly 200 by day^{-1} across the $p^*=500$ mb surface. An approximate profile of $F(p^*)$ during the disturbed period can be obtained simply by assuming that $F(0)$ is roughly equal to $F(0)$ during the undisturbed period. The resulting profile is shown in Fig. 13. Clearly cumulus convection is significant up to and above the 500-mb level.

Observational checks of the $F(p^*)$ profiles above the sea surface are more difficult. Few direct measurements of the fluxes of latent and sensible heat above the sea surface have been made over the open sea. Bunker (1960) and Bean *et al.* (1972) made direct flux measurements from aircraft in the vicinity of the BOMEX box during the summer of 1956 and the BOMEX period during 1969, respectively. Similar measurements were reported by Warner (1971) in the trade wind regime off the eastern Australian coast at latitude 16.51°S during the winter of 1966. Values of the flux taken from their papers are shown in Fig. 16 together with the profiles of $F(p^*)$ from Fig. 13. The values from Warner (1971) and Bean *et al.* (1972) compare favorably with our flux profiles. The values of Bunker (1960) show poor agreement. Some of the discrepancy may be due to differences in time and location, but a substantial portion must be a result of the instrumental limitations described by Bunker (1960). Unfortunately, these observational limitations were most severe for the latent heat flux, which is the major component of the flux of moist static energy in the BOMEX region. Rough agreement between a water vapor flux profile obtained by budget computations and direct measurements by NOAA aircraft has been reported by Holland (1972) for the undisturbed period.

Finally, we note that while dry turbulent transports dominate the vertical eddy flux in the lowest 50 mb and cumulus convection dominates above, the flux profiles are not markedly different in the two regimes in both the disturbed and undisturbed situations. This indicates that the transport processes in the well-mixed subcloud layer and the cloud layer are coupled and cooperate to increase the moist static energy of the trades.

6. Summary and conclusions

Large-scale mass, heat, and moisture budgets are examined using BOMEX data during 22–30 June 1969.

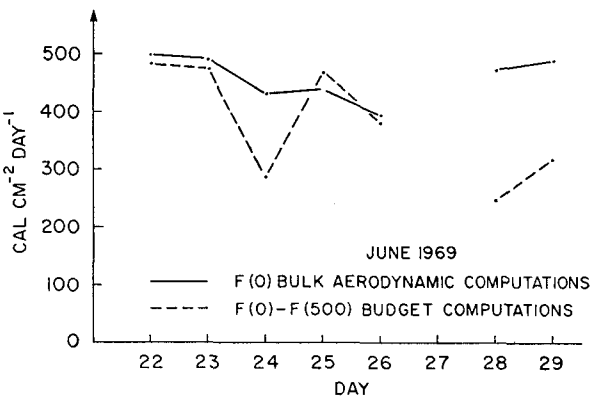

FIG. 15. $F(0)$ obtained by the bulk aerodynamic method and $F(0)$–$F(500)$ from the budget computations for each day.

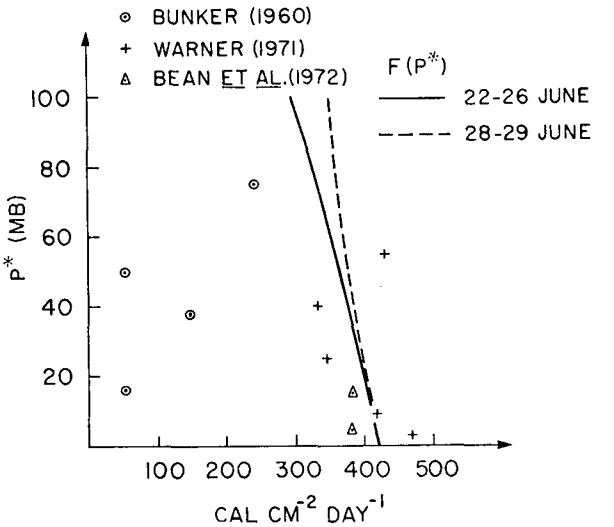

FIG. 16. Aircraft measurements of the vertical flux of moist static energy taken from Bunker (1960), Bean *et al.* (1972), and Warner (1971) and vertical profiles of $F(p^*)$ for the undisturbed (22–26 June) and the disturbed (28–29 June) periods obtained by large-scale budgets analysis.

With the aid of cloud photographs from ATS-3, the whole period is subdivided into two parts, i.e., an undisturbed period (22–26 June) and a disturbed period (28–29 June). During the undisturbed period, strong divergence exists in the lower layer, and downward motion and negative relative vorticity predominate in the whole layer below $p^*=500$ mb. A large apparent heat sink and apparent moisture source are found near the top of the trade inversion. In the upper layer, Q_1 and Q_2 tend to zero and this shows that there exist few clouds which penetrate this stable layer. Vertical eddy transport of total heat rapidly decreases near the trade inversion layer and is reduced to about 10% of total heat supply from the surface at $p^*=300$ mb. In general, the results during this period agree well with those obtained by Holland and Rasmusson (1973) and Augstein *et al.* (1973).

On the other hand, mass, heat and moisture budgets during the disturbed period are quite different from those during the undisturbed period. Low-level convergence and upward motion are observed during this period. Relative vorticity in the lower layer is near zero or slightly positive. Q_1-Q_R and Q_2 are positive in the layer below $p^*=300$ mb due to the warming and drying effects of compensating downward motion between clouds. Above $p^*=300$ mb, both Q_1-Q_R and Q_2 become negative due to detrainment effects of cumulus clouds. The total heat flux due to cumulus clouds is nearly constant from $p^*=80$ mb to $p^*=300$ mb. About 40% of the total heat flux at the surface penetrates the BOMEX upper boundary. Budgets on 28 June are more disturbed than on 29 June and this result coincides with that obtained from the satellite cloud photographs.

Evaporation from the ocean surface is computed by the bulk aerodynamic method. Sensible heat supply is estimated from the evaporation by assuming a constant Bowen ratio. During the undisturbed period, the total heat supply computed from the large-scale budgets agrees well with that obtained by the aerodynamic method. On the other hand, the total heat flux difference between the surface and $p^*=500$ mb is 200 ly day^{-1} less than the total heat supply from the surface obtained by the aerodynamic computation during the disturbed period. This difference is caused by the existence of upward heat flux due to cumulus clouds at $p^*=500$ mb.

Although the cloud cluster affecting the BOMEX region during the disturbed period only passes the southern boundary, the large-scale budgets for this period are very different from those of the undisturbed period. The effects of this cluster are very important for the large-scale budgets.

Finally, a comparison of the apparent heat source and moisture sink profiles of this trade wind region study and those of the ITCZ region studies of Yanai *et al.* (1973) and others shows that the average characteristics of the two regimes are strikingly different. This suggests that there will also be striking differences in the average spectra of cumulus clouds and the forcing mechanisms responsible for their maintenance. Studies of the cloud mass distribution function and the relation between cumulus clouds and mixed layer structure will be performed by the authors using BOMEX data.

Acknowledgments. The authors wish to express their thanks to Professor Michio Yanai for his encouragement throughout this work. We are indebted to CEDDA of NOAA, specifically to Dr. Eugene Rasmusson and Mr. Jason Ching, for providing the excellent rawinsonde and ship boom data used in this study. S. E. would also like to thank CEDDA for making possible a visit to inspect available data sets. We also thank Dr. D. N. Sikdar and Mrs. Jean Rickli of the University of Wisconsin for producing the enhancement, precision-display cloud photographs of ATS-3 during the analyzed period. The research reported here was supported by the National Science Foundation, Atmospheric Sciences Section (Grant GA-31694).

REFERENCES

Augstein, E., H. Riehl, F. Ostapoff and V. Wagner, 1973: Mass and energy transports in an undisturbed Atlantic trade-wind flow. *Mon. Wea. Rev.*, **101**, 101–111.

Bean, B. R., R. Gilmer, R. L. Grossman and R. McGavin, 1972: An analysis of airborne measurements of vertical water vapor flux during BOMEX. *J. Atmos. Sci.*, **29**, 860–869.

Bunker, A. F., 1960: Heat and water-vapor fluxes in air flowing southward over the western north Atlantic ocean. *J. Meteor.*, **17**, 52–63.

Chang, C.-P., 1970: Westward propagating cloud patterns in the tropical Pacific as seen from time-composite satellite photographs. *J. Atmos. Sci.*, **27**, 133–138.

Gray, W. M., 1972: Cumulus convection and large-scale circulations, Part III. Broad scale and meso scale considerations. Atmos. Sci. Paper No. 190, Colorado State University, 80 pp.

Holland, J. Z., 1972: Comparative evaluation of some BOMEX measurements of sea surface evaporation, energy flux and stress. *J. Phys. Oceanogr.*, **2**, 476–486.

——, and E. M. Rasmusson, 1973: Measurements of the atmospheric mass, energy, and momentum budgets over a 500-km square of tropical ocean. *Mon. Wea. Rev.*, **101**, 44–55.

Joint Organizing Committee, GARP, 1970: Report on the first session of the JOC Study Group on Tropical Disturbances, 1968, Appendix 1. *GARP Publ. Ser.*, No. 4.

Malkus, J. S., 1958: On the structure of the trade wind moist layer. *Papers Phys. Oceanogr. Meteor.*, **13**, No. 2.

Manabe, S., J. L. Holloway, Jr. and H. M. Stone, 1970: Tropical circulation in a time-integration of a global model of the atmosphere. *J. Atmos. Sci.*, **27**, 580–613.

Nitta, T., 1970: A study of generation and conversion of eddy available potential energy in the tropics. *J. Meteor. Soc. Japan*, **48**, 524–528.

——, 1972: Energy budget of wave disturbances over the Marshall Islands during the years of 1956 and 1958. *J. Meteor. Soc. Japan*, **50**, 71–84.

——, and S. Esbensen, 1973: Diurnal variations in the western Atlantic trades. (Submitted to *J. Meteor. Soc. Japan*).

Ostapoff, F., W. W. Shinners and E. Augstein, 1970: Some tests on the radiosonde humidity error. NOAA Technical Report ERL 194-AOML4, 50 pp.

Pond, S., G. T. Phelps, J. E. Paquin, G. McBean and R. W. Stewart, 1971: Measurements of the turbulent fluxes of momentum, moisture and sensible heat over the ocean. *J. Atmos. Sci.*, **28**, 901–917.

Reed, R. J., and E. E. Recker, 1971: Structure and properties of synoptic-scale wave disturbances in the equatorial western Pacific. *J. Atmos. Sci.*, **28**, 1117–1133.

Teweles, S., 1970: A spurious diurnal variation in radiosonde humidity records. *Bull. Amer. Meteor. Soc.*, **9**, 836–840.

Wallace, J. M., 1971: Spectral studies of tropospheric wave disturbances in the tropical western Pacific. *Rev. Geophys. Space Phys.*, **9**, 557–612.

Warner, J., 1971: Observations of the eddy fluxes of heat and vapour over the sea. *Quart. J. Roy. Meteor. Soc.*, **97**, 540–547.

Williams, K. T., 1970: A statistical analysis of satellite-observed trade wind cloud clusters in the western north Pacific. Atmos. Sci. Paper No. 161, Colorado State University, Fort Collins, 80 pp.

Yanai, M., S. Esbensen and J.-H. Chu, 1973: Determination of bulk properties of tropical cloud clusters from large-scale heat and moisture budgets. *J. Atmos. Sci.*, **30**, 611–627.